fluids

MDPI

Article

Numerical Investigation of High-Reynolds-Number Air-Ventilated Water Flow under Solid Body with Surface Geometry Variations

Konstantin I. Matveev * and Jeffrey M. Collins

School of Mechanical and Materials Engineering, Washington State University, Pullman, WA 99164, USA; jeffrey.m.collins@wsu.edu

* Correspondence: matveev@wsu.edu

Abstract: Air-ventilated cavities formed under or around the hulls of marine vehicles can reduce water drag. Hull configurations with partial air ventilation where air cavities reattach to body surfaces are of special practical interest, since the required air supply rates to achieve significant drag reduction can be made rather low. However, formation and stability of such air cavities are sensitive to the hull geometry and operational conditions. In this study, an attempt is made to numerically simulate one setup with a partial air cavity that was previously tested experimentally at high Reynolds numbers, above 50 million. A computational fluid dynamics software Star-CCM+ has been employed for numerical modeling. Stable and unstable states of the air-cavity setup, characterized by long and collapsing air cavities, respectively, were modeled at two air supply rates near the stability boundary. Numerical results were similar to experimental data at the optimal water speed for the tested geometry, when a long air cavity was sustained at a minimal air supply rate. For water speeds that were substantially higher or lower than the optimal case, a stable cavity could not be maintained with small air supply rates for the given hull geometry. Numerical simulations demonstrated how alterations of the body surface could help sustain long air cavities across a broader speed range using air supply rates that were similar to the optimal case. These findings suggest that morphing hull surfaces can potentially be used for control of drag-reducing air cavities and expand the viable operating range for their application to marine vehicles.

Keywords: drag reduction; air-ventilated water flow; computational fluid dynamics; stability

Citation: Matveev, K.I.; Collins, J.M. Numerical Investigation of High-Reynolds-Number Air-Ventilated Water Flow under Solid Body with Surface Geometry Variations. *Fluids* **2021**, *6*, 174. https://doi.org/10.3390/fluids6050174

Academic Editor: Byoung-Kwon Ahn

Received: 8 April 2021
Accepted: 24 April 2021
Published: 29 April 2021

1. Introduction

Reducing water drag of marine vehicles is critical for both marine transportation and naval applications, since it can lead to more economically efficient and faster vessels. One technique for decreasing frictional water drag involves air injection on the underwater hull surfaces. If stable air cavities of large-area can be maintained at low air supply rates near the solid surface, water drag and vehicle power consumption can decrease significantly. While there are a variety of air-assisted methods for drag reduction, such as using small air bubbles [1] and thin air layers [2], the topic of the present paper is limited to bulkier air cavities with small air leakage. It should be noted that naturally occurring air ventilation under stepped hull surfaces can also reduce hydrodynamic drag [3,4], but this method can be realized only on high-speed boats planing on the water surface.

The idea for the air-cavity drag reduction originated in the 19-th century [5], and several air-cavity boats were built [6,7]. However, due to issues with formation and stability of large air cavities at economical air supply rates and a lack of numerical tools for confident design of such systems, the broad implementation of air-cavity ships has not yet occurred. One major problem is the complexity of physical phenomena [8,9] related to wall-bounded, turbulent, multi-phase flows, occurring in the presence of gravity and often in unsteady environments. Another issue is the importance of scale effects. While

the air cavity shape is mainly influenced by Froude number and ventilation (or cavitation) number, the air leakage rates are also affected by Reynolds and Weber numbers. The influence of Weber number can be minimized at a reasonable size of small-scale models, but it is difficult to achieve similar Reynolds number in experiments with small models of ship hulls.

To ensure well developed turbulent flow on scaled models, especially when multi-phase phenomena are important, it is desirable to test them in high-Reynolds number regimes with Re well above 10^7. Alternatively, one can use turbulence stimulators on the front part of the body surface. To provide experimental data for high-Re air-ventilated water flows under a solid hull, experiments involving long (>10 m) models were conducted in the world's largest cavitation tunnel several years ago [10]. The tested hull was a streamlined body with a recess incorporated on the lower surface to accommodate a partial air cavity that re-attaches at the sloping hull surface ("beach") in the aft part of the body (Figure 1a). The corresponding Reynolds numbers in these tests were above 5×10^7.

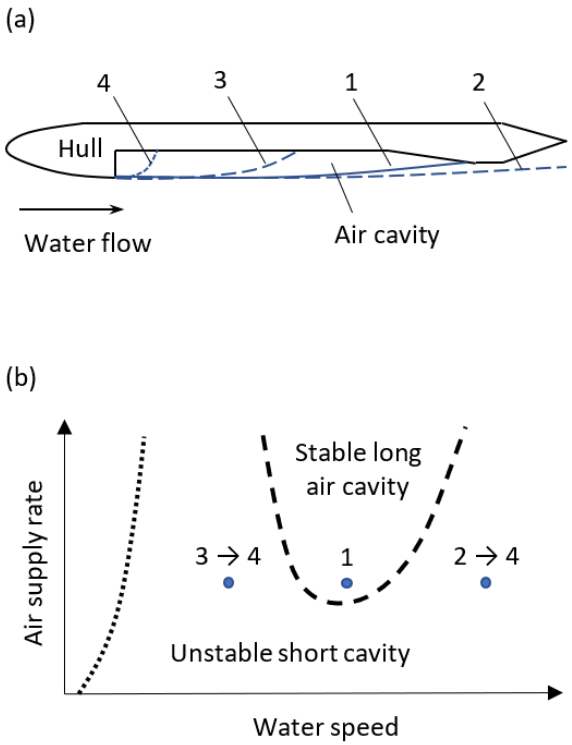

Figure 1. (**a**) Schematic of the recessed hull form (not-to-scale; vertical dimensions are exaggerated). Solid blue line 1, boundary of stable cavity at optimal water speed; dashed line 2, nominal air cavity at higher speed (unstable at low air supply); dashed line 3, nominal air cavity at lower speed (unstable at low air supply); dotted line 4, collapsed short air cavity. (**b**) Stability boundaries for long air cavity in the recessed hull setup. Dashed line shows stability boundary in the speed range of interest. Dotted line shows expected stability boundary at very low speeds.

A typical dependence of the stability boundary between stable states with long cavities and collapsed cavities is shown by a dashed line in Figure 1b in terms of air flow rate and incident water flow velocity. There is an optimal water speed (or a narrow speed range) at which the required air supply is minimal (state 1 in Figure 1). In this condition, the cavity boundary meets the rear section of the body without large flow disturbances. The rise of the air–water interface behind the upstream step in this setup is similar to that in a gravitational surface wave. Previous potential-flow calculations indicated that a smooth attachment of the cavity behind a step under an infinite horizontal wall is about 0.4 of the gravitational wavelength ($\lambda = 2\pi U^2/g$) of the two-dimensional surface water

wave behind a body moving with velocity U in deep water [11]. If the water speed in the considered configuration is higher than optimal, then the air-cavity interface would tend to go under (overshoot) the rear section of the body (nominal state 2 in Figure 1), and the loss of air would be very large since there is no solid surface downstream to which the cavity can reattach. This regime is similar to superventilated regimes of underwater objects. In the case of a water speed sufficiently lower than optimal (nominal state 3 in Figure 1), the boundary of a shorter cavity would approach the recess ceiling at a large angle, resulting in a rough impingement with formation of a re-entrant jet which also causes a large air leakage. Therefore, cavity shapes 2 and 3 will not exist at reasonably small air supply rates and would instead collapse down to a short cavity behind the step as shown by shape 4 in Figure 1a. The experimental curve for the stability boundary exhibits steep increases in the air supply when the water speed deviates from the optimal condition (Figure 1b).

It should be noted that at zero or very low speeds of water flow, an air cavity can exist in the top portion of the recessed space. The stability boundary for this regime is schematically shown by a dotted line in Figure 1b. However, the back side of the step will be partially wetted at such low speeds and drag reduction benefits may not be even present in this case. This situation with very low speeds was not investigated by Lay et al. [10] and is not considered in this study.

Effects similar to those described above can be also expected on realistic ship hulls with air-cavity systems. Hence, performance of air-cavity ships would be near optimal only in a narrow range of operational situations. Since ship speeds and loading conditions vary in practice, and sea-going ships often experience significant motions in waves, it will be desirable to have some means for controlling air-ventilated flows to maximize air cavity sizes and maintain drag savings in a broad range of conditions. Simplified consideration and discussion of static and active control means for air cavity systems were reported [12–14].

Early efforts on computational modeling of air-cavity systems, such as described above, were based on the potential flow theory [11,15,16]. While these methods ignore viscous effects, they can approximately predict the air cavity shapes and be used in the preliminary design of air-cavity hulls. More comprehensive computational fluid dynamics (CFD) programs, which include viscosity, turbulence phenomena, surface tension and other effects, have been also applied for modeling air-cavity systems, but primarily at relatively moderate Reynolds numbers corresponding to most laboratory experiments [17–19]. Obtaining good agreement even at such Reynolds numbers is still a challenging task. Some recommendations for numerical settings include usage of a very fine mesh in the region of cavity reattachment to a solid surface and utilizing a sharpening treatment in the interface-capturing scheme [20].

The main objectives of the present study are two-fold. First, an attempt is made to use the state-of-the-art CFD code Star-CCM+ to reproduce stable and unstable states of air cavities recorded in high-Re experiments by employing economical numerical settings (two-dimensional setup with Reynolds-averaged Navier–Stokes approach). Second, geometric modifications of the body lower surface are sought that can extend the range of water speeds at which large air cavities exist at low air supply rates. Thus, the present work aims to demonstrate how CFD can potentially assist in the development of adaptive air-cavity systems with relatively low computational cost.

2. Computational Modeling Aspects

Numerical simulations of air-ventilated water flows were carried out with CFD software STAR-CCM+ (Siemens, Munich, Germany). It employs a finite-volume segregated viscous solver. The second-order discretization in space and the first-order implicit stepping in time were utilized here [21]. Flows of constant-density water and ideal-gas air were modeled within the Eulerian multiphase framework based on the volume-of-fluid (VOF) method [22]. Surface tension and gravity were also included.

The employed Reynolds-averaged Navier–Stokes equations (RANSE) approach includes the governing transport equations for the continuity and momentum,

$$\frac{\partial \rho}{\partial t} + \frac{\partial (\rho u_j)}{\partial x_j} = 0 \tag{1}$$

$$\frac{\partial (\rho u_i)}{\partial t} + \frac{\partial (\rho u_i u_j)}{\partial x_j} = -\frac{\partial p}{\partial x_i} + \frac{\partial}{\partial x_j}\left[\mu\left(\frac{\partial u_i}{\partial x_j} + \frac{\partial u_j}{\partial x_i} - \frac{2}{3}\delta_{ij}\frac{\partial u_k}{\partial x_k}\right) - \rho\overline{u'_i u'_j}\right] + \rho f_i \tag{2}$$

where u_i is the Reynolds-averaged velocity, p is the pressure, ρ is the mixture density, f is the body force, and $-\rho\overline{u'_i u'_j}$ is the Reynolds stress. The effective density ρ and viscosity μ are computed as $\rho = \rho_a\beta + \rho_w(1-\beta)$ and $u = u_a\beta + u_w(1-\beta)$, where β is the air volume fraction, and indices a and w stand for air and water, respectively. The Boussinesq hypothesis gives the expression for the Reynolds stresses,

$$-\rho\overline{u'_i u'_j} = \mu_t\left(\frac{\partial u_i}{\partial x_j} + \frac{\partial u_j}{\partial x_i} - \frac{2}{3}\delta_{ij}\frac{\partial u_k}{\partial x_k}\right) - \frac{2}{3}\rho k\delta_{ij}, \tag{3}$$

where μ_t is the turbulent viscosity and k is the turbulent kinetic energy.

In most cases considered in this work, the all-Y+ realizable $k-\varepsilon$ model was employed [23], as it showed promising results in previous simulations at lower Reynolds numbers [20]. The all-Y+ SST (shear stress transport) $k-\omega$ model was also tried as noted in the next section. In the realizable $k-\varepsilon$ model, governing equations for the turbulent kinetic energy k, the turbulent dissipation rate ε, and the turbulent viscosity μ_t are represented as follows,

$$\frac{\partial (\rho k)}{\partial t} + \frac{\partial (\rho k u_j)}{\partial x_j} = \frac{\partial}{\partial x_j}\left[\left(\mu + \frac{\mu_t}{\sigma_k}\right)\frac{\partial k}{\partial x_j}\right] + G_k - \rho\varepsilon, \tag{4}$$

$$\frac{\partial (\rho k)}{\partial t} + \frac{\partial (\rho k u_j)}{\partial x_j} = \frac{\partial}{\partial x_j}\left[\left(\mu + \frac{\mu_t}{\sigma_k}\right)\frac{\partial k}{\partial x_j}\right] + G_k - \rho\varepsilon, \tag{5}$$

$$\frac{\partial (\rho\varepsilon)}{\partial t} + \frac{\partial (\rho\varepsilon u_j)}{\partial x_j} = \frac{\partial}{\partial x_j}\left[\left(\mu + \frac{\mu_t}{\sigma_\varepsilon}\right)\frac{\partial \varepsilon}{\partial x_j}\right] + \rho C_{\varepsilon 1} S\varepsilon - \rho C_{\varepsilon 2}\frac{\varepsilon^2}{k + \sqrt{\nu\varepsilon}}, \tag{6}$$

where G_k is the turbulent production, S is the modulus of the mean strain rate, ν is the kinematic viscosity, and σ_k, σ_ε, $C_{\varepsilon 1}$, $C_{\varepsilon 2}$, C_μ are the model coefficients [24].

One should keep in mind several limitations of the present approach. Although numerically economical, the RANSE approximation does not allow us to accurately resolve turbulent fluctuations that can be important for air-ventilated flows, especially at the cavity tail, where air sheds from the cavity in form of air pockets and bubbles. Possibly problematic properties of the realizable $k-\varepsilon$ model employed here include over-prediction of eddy-viscosity and assumption of the isotropic turbulence at the cavity interface [25]. Detached Eddy Simulation and Large Eddy Simulation modeling approaches can increase the simulation fidelity but will require large computational resources [26].

For the current simulations of air-ventilated water flows, geometry of an elongated body from the high-Re experiments reported by Lay et al. [10] is utilized. The test model spans the water channel that is 3.05 m wide and 3.05 m tall. Here, this model is treated as a two-dimensional body. Its sectional view and main dimensions are shown in Figure 2. More detailed geometry is described by Lay et al. [10], but some important parameters include the following: the body length is 12.90 m; the sloped beach is 2.77 m long and has an angle of 1.21° with respect to a horizontal plane; and the forward step height near the air injector is 90 mm. All results reported in this paper were obtained in two-dimensional simulations, since we aimed at exploring whether two-dimensional (2D) simulations would be able to capture existence and collapse of long air cavities. The three-dimensional (3D)

modeling of this experiment would require very big computational resources unavailable to us in this study.

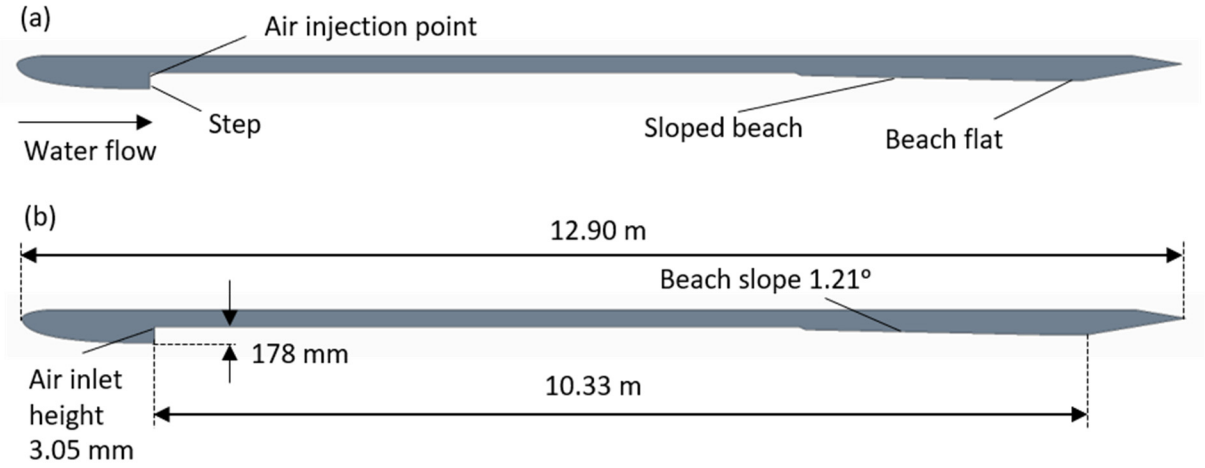

Figure 2. (**a**) Geometry and (**b**) dimensions of body with recess on the lower side.

The 2D setup and limited mesh resolution inevitably lead to simplifications of the complex air leakage process, which may involve shedding of clusters of small bubbles. The expected 3D effects include non-uniform flow features in the transverse direction within the cavity re-attachment region, as observed in the experiments by Lay et al. [10]. The surface tension effects on the formation and dynamics of small air bubbles will be stronger in the 3D formulation. The flow will be also affected by side boundaries of the water channel. The 3D effects often result in predominant air leakage near the edges of the recess on actual air-cavity boats [6], although boat hull geometries also have much more pronounced 3D structural features than the currently simulated experiment. Nevertheless, one of our goals in this study was to check whether a transition between different flow regimes (from a long stable cavity to a collapsed cavity) can be adequately predicted with the present two-dimensional approach at least in a simple geometry.

The numerical domain is selected to represent the longitudinal-plane test section of the water tunnel (Figure 3). In simulations, the body surface and the top and bottom walls of the channel are treated as no-slip walls. The upstream and downstream boundaries of the domain are represented by the velocity inlet and the pressure outlet, respectively. There is also a small air inlet on the back side of the step near the ceiling (Figure 2). The height of the air inlet is 3.05 mm, which is much smaller than the step height.

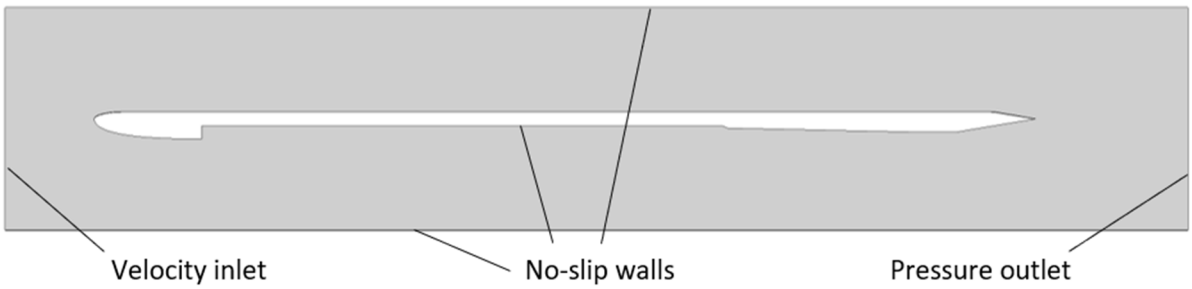

Figure 3. Numerical domain and boundary conditions.

The numerical mesh comprised primarily of quadrilateral cells was built in the domain (Figure 4). Prismatic layers with 10 cells across were formed near the top and bottom channel walls and wetted sections of the test model. The near-wall cell thickness was selected to ensure Y+ values of 30–80, thus relying on the wall function approach to model

the water boundary layer. In the area where the air was present (i.e., in the recesses zone from the step to the trailing edge), a denser mesh with primarily square cells was generated having about 20 cells across the step height for the fine mesh used in this study. The simplified modeling of boundary layers, especially within the cavity reattachment region, can only approximately resolve fine features of wall-bounded turbulent flow and complex multi-phase processes in the present setup, such as detachment of air bubbles from the cavity tail and re-establishment of the boundary layer behind the air cavity. The main motivation for using the wall function approach was to explore if one can still capture macroscopic characteristics of the studied flow with economical numerical settings. The time step in simulations was selected to keep the Courant number around 0.5.

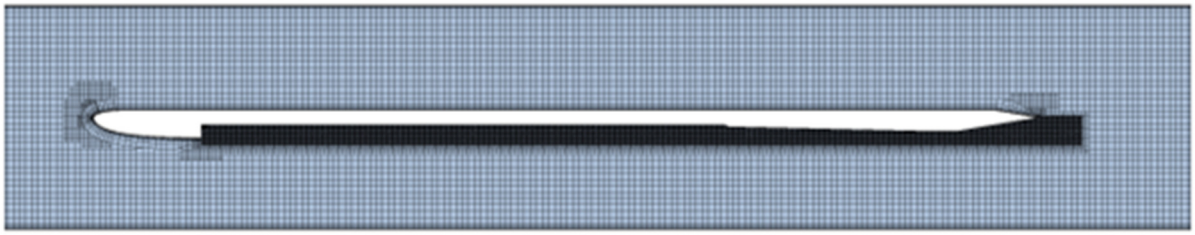

Figure 4. Numerical mesh in the fluid domain.

3. Results

The numerical simulations were conducted in a manner similar to the experimental sequence. First, a large air flow rate was assigned to fill the recessed zone with air. In this state, the air cavity shed large air pockets shedding downstream. Then, the air supply rate was gradually reduced so the cavity reattached to the body in the beach region (shape 1 in Figure 1). In this regime, only small air pockets detached from the air cavity. With further reduction of the air supply rate, a stable cavity could no longer be maintained. It relatively quickly collapsed to form a very short cavity on the back side of the step (cavity 4 in Figure 1). Predicting this critical air supply rate, i.e., the minimal rate needed to maintain the air cavity, is of major importance for practical applications.

The initial CFD simulations were conducted at the incident water speed of 5.4 m/s, near the optimal condition in the experiments of Lay et al. [10], when the minimal air supply rate needed to maintain a large air cavity was found in the tests to be to the range 0.012–0.018 in terms of the non-dimensional air flow rate, defined as

$$q = \frac{Q}{hbU}, \tag{7}$$

where Q is the actual dimensional air supply rate, U is the incident water flow velocity, h and b are the step height and beam, respectively. At this speed, the Reynolds number based on the water properties and the hull length is about 7.8×10^7.

Since more experimental data points were clustered around $q = 0.016$ [10], this condition (together with water speed 5.4 m/s) was selected for the mesh-independence study in this work. Three numerical grids (coarse, medium and fine) were generated. As the metrics of convergence, the following parameters were used: the air cavity length L_c, measured from the step to the cavity reattachment point, and the drag coefficient C_D, defined as follows,

$$C_D = \frac{F}{0.5\rho_w U^2 L}, \tag{8}$$

where F is the two-dimensional drag force on the body, ρ_w is the water density, and L is the body length.

The computational results for the cavity lengths and drag coefficients for different grids are given in Table 1. They demonstrate monotonic numerical convergence with the mesh refinement. The air cavities obtained on the fine and medium grids can be considered

as stable long cavities, while the case with the coarse mesh leads to the cavity collapse. Illustrations of the cavity shapes found using the fine and coarse grids are shown in Figure 5. The coarse-mesh air cavity occupies a very small region near the air inlet. This confirms previous findings that a sufficiently fine mesh in the recess region is critically important for modeling hulls with air cavities. The drag coefficient results show that drag of the hull with an air cavity is about twice smaller than the drag of the body with almost completely wet surface (Table 1).

Table 1. Results obtained in mesh-dependency study at $q = 0.016$ and $U = 5.4$ m/s.

Mesh	Cell Count	Air Cavity Length, m	Drag Coefficient
Coarse	25734	0.31	0.01160
Medium	32221	9.81	0.00552
Fine	44522	10.30	0.00521
Numerical uncertainty		0.03	0.00002

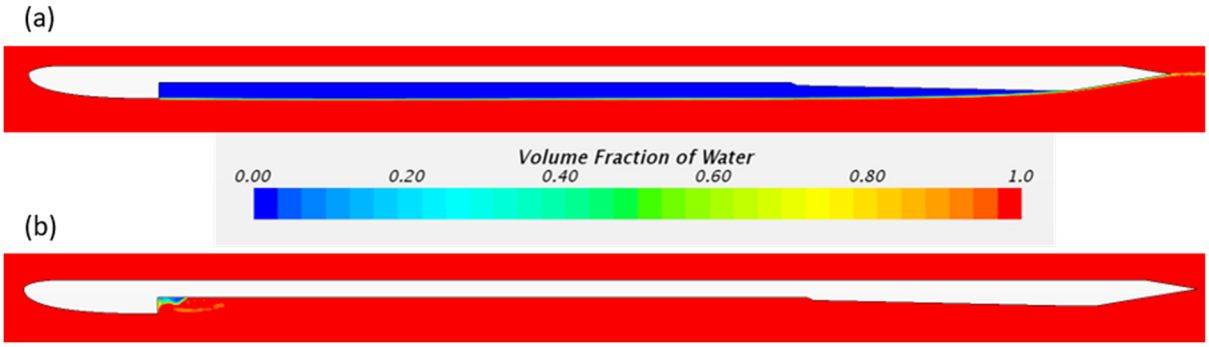

Figure 5. Air cavity views in steady-state regimes at $q = 0.016$ and $U = 5.4$ m/s obtained on (**a**) fine mesh and (**b**) coarse mesh.

To assess numerical uncertainties for the cavity length and drag coefficient, the Richardson extrapolation was employed to determine expected corrections δ_{RE} to the fine-mesh solutions [21],

$$\delta_{RE} = \frac{\Delta_{12}}{\beta^p - 1}, \tag{9}$$

$$p = \frac{\log(\Delta_{23}/\Delta_{12})}{\log(\beta)}, \tag{10}$$

where Δ_{12} is the difference between solutions obtained on the fine and medium grids, Δ_{23} is the solution difference on the medium and coarse grids, β is the grid refinement ratio, and p is the observed accuracy order. Then, safety factors are applied towards δ_{RE} to obtain numerical uncertainties [27], which are listed in Table 1. These uncertainties are below 1% of the values for the cavity length and drag coefficient obtained on the fine mesh, and therefore, they are deemed acceptable for the present study.

For illustrative purposes, velocity streamlines and magnitudes obtained on the fine mesh are depicted in Figure 6. One can notice that the water flow by-passes the hull and air cavity as a singular object, so the air cavity boundary resembles a nearly drag-free surface. The water re-attaches to the hull in the stern portion. The air flow in the recessed zone forms two vortices: a short vortex near the air inlet on the back side of the step, where speeds are moderate, and a very long vortex that occupies most of the cavity, where velocities are low.

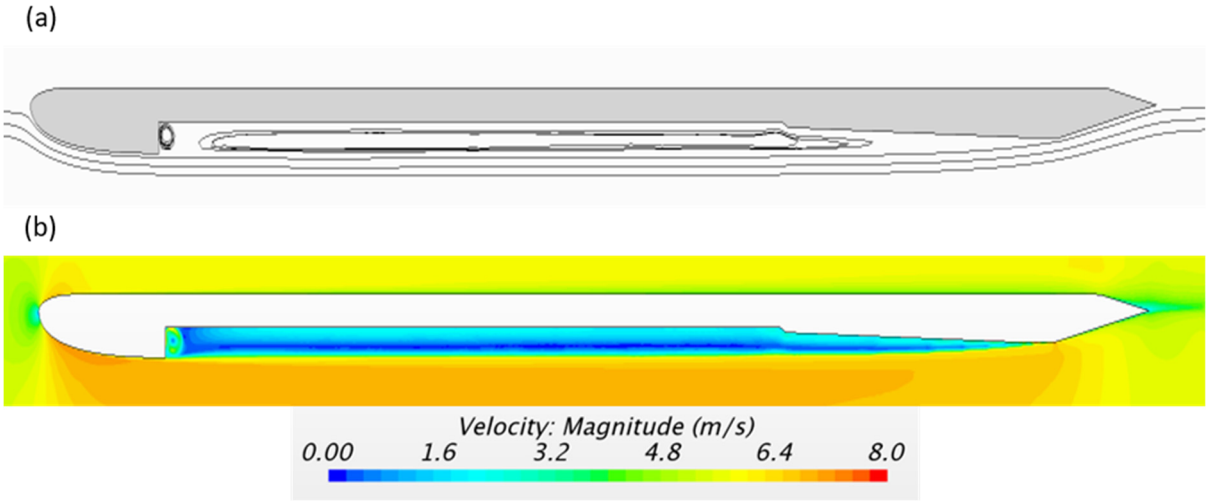

Figure 6. (**a**) Streamlines and (**b**) velocity magnitudes for numerical solution obtained on fine mesh at q = 0.016 and U = 5.4 m/s. Vertical dimensions are scaled up two times for clarity.

In order to compare numerical results for the minimum air supply rate needed to maintain the air cavity, the air flow rate was further reduced down to q = 0.010 (the incremental variation in the air flow magnitude was similar to experimental scatter of critical air flow rates). Since the air leakage from the air cavity in the stable state was greater than the air supply, the cavity started contracting and eventually collapsed. Images of the air cavity in the middle of this process and near the end are shown in Figure 7. Reattachment of the cavity to the recess ceiling at this water speed was not smooth, and the air detached from the cavity in the form of large pockets during collapse. Flow streamlines and the velocity magnitude field are shown in Figure 8, which corresponds to Figure 7b. In contrast to the case with the air-filled recess (Figure 6), the recirculation zone behind the step was now short, and the water streamlines quickly approached the recess ceiling producing a larger shear rate along almost entire ceiling surface. In the collapsed steady state, the body drag coefficient more than doubled (C_D = 0.0114).

The superposition of experimentally determined minimum air supply rates required to maintain long air cavities and air flow rates used in the current numerical simulations are given in Figure 9. From these results, it can be concluded that a numerical prediction for the minimum air supply needed to maintain a long stable cavity belonged to the non-dimensional air flow rate range of 0.010–0.016, whereas experimental data points indicated that transition to instability happened for q being between 0.012 and 0.018. Therefore, a satisfactory agreement between CFD and test results for the stability boundary was found in the studied conditions.

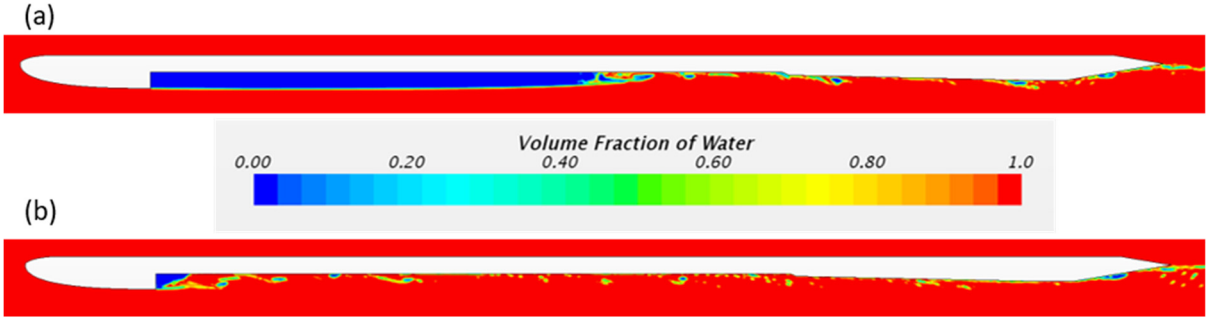

Figure 7. Air cavity in the collapsing process when air supply was reduced from q = 0.016 to 0.010. Cavity shapes: (**a**) intermediate state, (**b**) close to the completely collapsed state.

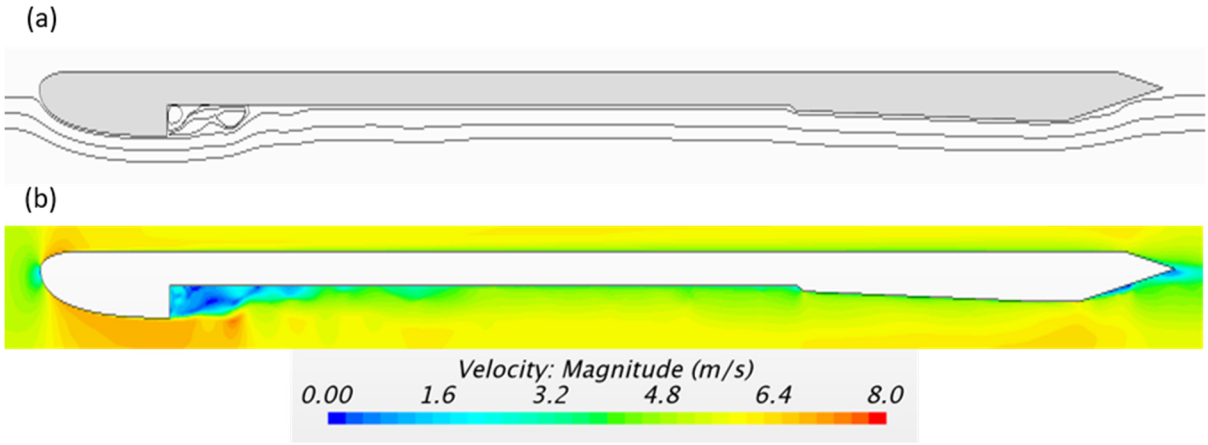

Figure 8. (**a**) Streamlines and (**b**) velocity magnitudes in the state close to complete air-cavity collapse (as in Figure 7b) at $q = 0.010$ and $U = 5.4$ m/s. Vertical dimensions are scaled up two times for clarity.

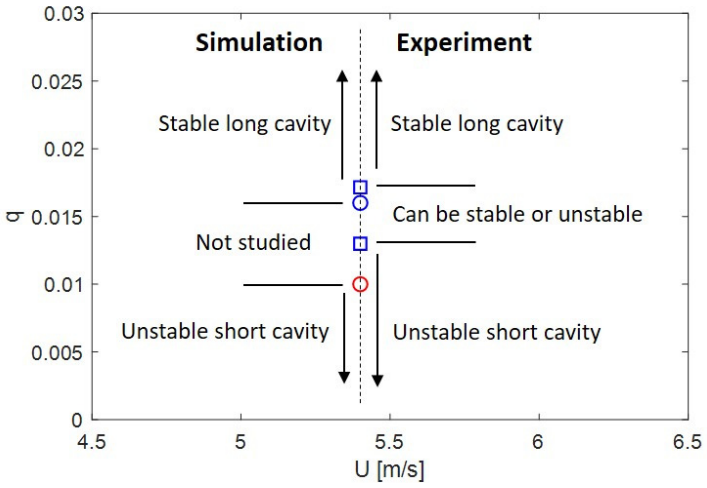

Figure 9. Air cavity regimes near water speed 5.4 m/s. Blue squares, experimentally obtained minimum air flow rates required to maintain stable long air cavity. Blue circle, numerically used air flow rate when stable long air cavity was present (as in Figure 5a). Red circle, numerically used air flow rate when air cavity collapsed to short state (as in Figure 7b).

In order to check the sensitivity of numerical simulations to the chosen turbulence model, SST $k - \omega$ with all-Y+ treatment was also used for modeling the air cavity at the incident water speed $U = 5.4$ m/s. In case of the non-dimensional air flow rate $q = 0.016$, a stable long cavity was maintained, and for $q = 0.010$ the cavity collapsed similar to the previously described case. Thus, no significant difference in results for the stability boundary obtained was detected with a different turbulence model.

As discussed previously, a long stable cavity in the experimental setup could only be maintained at low air supply rates within a narrow speed range [10]. Increasing and decreasing water speed by 50% in the present simulations also showed that a long cavity could not be sustained at $q = 0.016$. In order to broaden the speed range where a long air cavity was present (which is of great practical interest), relatively small modifications in the body shape could be sought.

Since it is expected that increasing the incident water speed would make the air cavity overshoot the beach (Figure 1a), two strategies can be explored. One is to modify or "trim" the step (Figure 10a) so that the cavity surface elevation at the originating step edge would approach vertical position of the stern section. Such a modification was suggested previously for suppressing water surface amplitudes under air-cavity hulls

with long recesses [28] and is also related to selecting stern geometries of conventional ship hulls [29]. In the modification explored here (Figure 10a), the step edge was moved up by a distance equal to 17% of the step height, and the angle of this cut was about 5.8° with respect to the horizontal plane. Another approach for minimizing the air cavity overshoot at higher speeds is to move the beach section down (Figure 10b). For this purpose, the second modification involved shifting the flat section of the beach down by about 50% of the difference between vertical positions of the step and the beach flat. To avoid producing a large slope on the beach inclined section, the beach was also extended forward (Figure 10b).

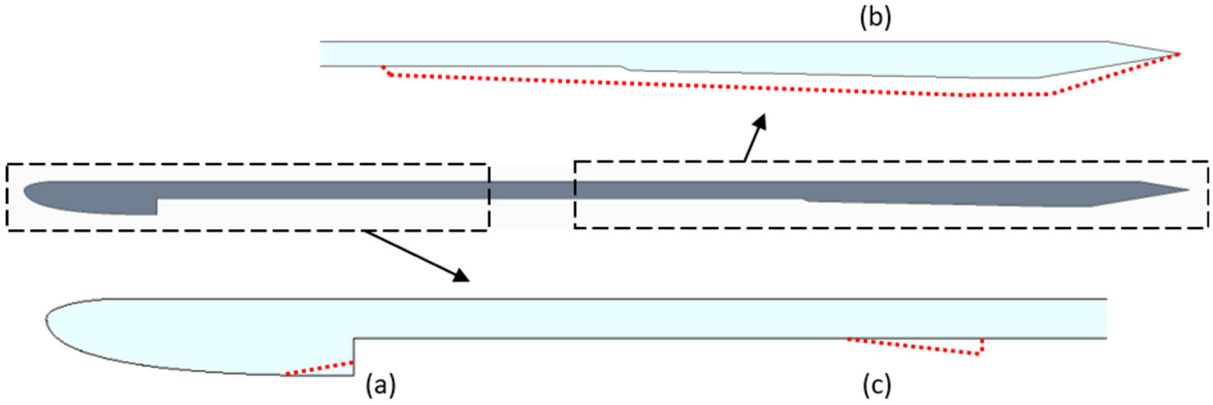

Figure 10. Body shape modifications (shown as dotted red lines) aimed at maintaining long air cavities: (**a**) step trimming for higher speed, (**b**) beach augmentation for higher speed, (**c**) intermediate wedge step for lower speed. Original body form is shown in the middle.

In case of lower speeds, the air-cavity length would shorten. To keep a large area of the hull covered with air cavities in numerical simulations, an additional wedge-type step was introduced on the cavity ceiling (Figure 10c), which was expected to accommodate two shorter air cavities on the otherwise unmodified original body configuration. The step angle was selected as 2.8°. The motivation for using a wedge was that it extended the length of the front air cavity [11], while serving as an anchor for inception of the next air cavity behind it. The air leakage from the first cavity provided air supply for the second cavity. This approach can be also related to older designs of air-cavity hulls (e.g., Pavlov et al. 2020), where intermediate steps were considered as assistance means to help form a large multi-wave air cavity as the ship was accelerating from rest to a design speed.

The first two body modifications were simulated with CFD at speeds 8.1 m/s (50% higher than previously used 5.4 m/s) and the third modification was studied at 2.7 m/s (50% lower than 5.4 m/s). A similar air supply strategy was employed: high air flow rate was assigned initially, and then gradually reduced after a formation of a large cavity. The steady-state air-cavity shapes obtained in simulations are shown in in Figure 11. In the first and third cases (Figure 11a,c), the original minimum air supply rate $q = 0.016$ was sufficient to maintain the air cavity, while a somewhat larger air flow rate $q = 0.024$ was required in the second case with the beach augmentation (Figure 11b). Thus, the considered here hull modifications presented viable means for expanding a speed range for recessed hulls in which long air cavities could be maintained.

A comparison of drag coefficient values for the modified configurations with air cavities and the original setup without air cavity is shown in Table 2. At lower speed of 2.7 m/s, the modified system with two air cavities (Figure 11c) had twice lower drag in comparison with the body with no added wedge and no air cavity, which clearly demonstrated an advantage of introducing this appendage. At higher speed of 8.1 m/s, the setup with a trimmed step (Figure 11a) also has almost twice lower drag than the original body with no cavity. In the third modification (Figure 11b), the augmented beach helped

maintain of a long cavity, but drag of this system was only marginally lower than that of the initial body with no air cavity (Table 2), which was caused by wider wake behind the modified body with an expanded stern section.

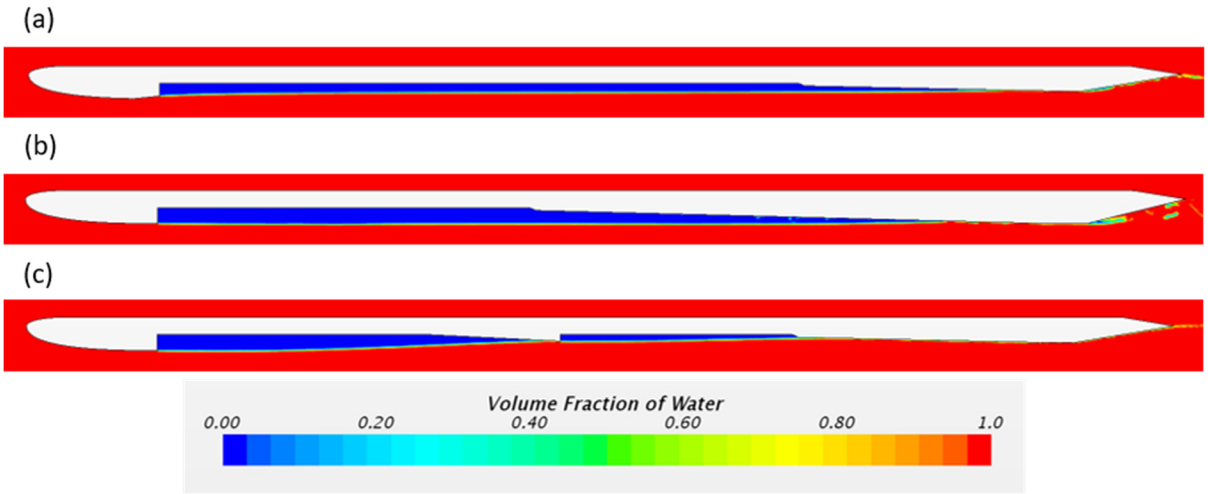

Figure 11. Stable air cavities under modified hulls: (**a**) with trimmed step at U = 8.1 m/s and q = 0.016, (**b**) with augmented beach at U = 8.1 m/s and q = 0.024, (**c**) with intermediate step at U = 2.7 m/s and q = 0.016. More detailed views of geometric modifications of the hull are given in Figure 10.

Table 2. Drag coefficients of original and modified configurations.

Configuration	Drag Coefficient
Speed 2.7 m/s	
Original setup, no air cavity (Figure 2)	0.01155
With intermediate wedge, split air cavity (Figure 9c)	0.00518
Speed 8.1 m/s	
Original setup, no air cavity (Figure 2)	0.01100
With trimmed step, long air cavity (Figure 9a)	0.00558
With augmented beach, long air cavity (Figure 9b)	0.01080

Therefore, at speed U = 8.1 m/s, the trimmed step seemed to be a better solution than beach augmentation for maintaining a long air cavity, due to both smaller air supply requirements and reduced drag. However, there was also a practical concern associated with thinner air cavities. In the presence of disturbances, which may be caused by sea waves and hull motions, thinner cavities will be more susceptible to disintegration. In some of air-cavity ship designs, the recess height is intentionally increased to maintain air cavities in disturbed environments. Investigation of the effects caused by unsteady incident water flow and hull motions on the requirements for air-cavity maintenance represent an interesting topic for future research but is beyond the scope of the current study.

4. Conclusions

The present study has demonstrated that 2D CFD simulations can adequately predict macroscopic features of high-Reynolds number air-ventilated water flows under a hull with a recess on its bottom. Using the numerically economical RANSE approach and a sufficiently fine mesh in the cavity region, approximate agreement with experimental data was obtained for the minimal air supply rate needed to maintain a long stable cavity. This shows promise for using commercial CFD tools for design of air-cavity hulls at realistic dimensions.

The second objective of this study was to show how modifications of the body surface can expand the range of hull speeds at which long air cavities can be maintained at reasonably low air supply rates. Specifically, a trimmed step and an augmented beach were utilized to fit the body geometry to flatten the air cavity surface at higher speeds, whereas an intermediate step was placed on the recess ceiling to assist formation of two shorter air cavities at lower speed. These findings suggest an opportunity for implementing morphing hull surfaces or compact actuators to augment and control air cavities. Computational modeling of air-ventilated flows in unsteady environments and exploring actively controlled surfaces and actuators for maintaining large air cavities are recommended as important topics for future research that would help broaden implementation of air-cavity systems on marine vessels.

Author Contributions: Conceptualization, J.M.C.; methodology, K.I.M.; formal analysis, K.I.M. and J.M.C.; investigation, K.I.M. and J.M.C.; resources, K.I.M.; writing—original draft preparation, K.I.M.; writing—review and editing, J.M.C.; visualization, J.M.C.; project administration, K.I.M.; funding acquisition, K.I.M. Both authors have read and agreed to the published version of the manuscript.

Funding: This research was funded by the U.S. National Science Foundation, grant number 1800135. The APC was funded by the U.S. National Science Foundation.

Institutional Review Board Statement: Not applicable.

Informed Consent Statement: Not applicable.

Data Availability Statement: The data presented in this study are available on request from the corresponding author.

Conflicts of Interest: The authors declare no conflict of interest.

References

1. Kawakita, C.; Sato, S.; Okimoto, T. Application of simulation technology to Mitsubishi air lubrication system. *Mitsubishi Heavy Ind. Tech. Rev.* **2015**, *52*, 50–56.
2. Elbing, B.R.; Winkel, E.S.; Lay, K.A.; Ceccio, S.L.; Dowling, D.R.; Perlin, M. Bubble-induced skin-friction drag reduction and the abrupt transition to air-layer drag reduction. *J. Fluid Mech.* **2008**, *612*, 201–236. [CrossRef]
3. Makasyeyev, M.V. Numerical modeling of cavity flow on bottom of a stepped planing hull. In Proceedings of the 7th International Symposium on Cavitation, Ann Arbor, MI, USA, 16–20 August 2009.
4. De Marco, A.; Mancini, S.; Miranda, S.; Scognamiglio, R.; Vitiello, L. Experimental and numerical hydrodynamic analysis of a stepped planing hull. *Appl. Ocean Res.* **2017**, *64*, 135–154. [CrossRef]
5. Latorre, R. Ship hull drag reduction using bottom air injection. *Ocean Eng.* **1997**, *24*, 161–175. [CrossRef]
6. Matveev, K.I. Modeling of vertical plane motion of an air cavity ship in waves. In Proceedings of the 5th International Conference on Fast Sea Transportation, Seattle, WA, USA, 31 August–2 September 1999.
7. Pavlov, G.A.; Yun, L.; Bliault, A.; He, S.-L. *Air Lubricated and Air Cavity Ships: Development, Design and Application*; Springer: New York, NY, USA, 2020.
8. Arndt, R.E.A.; Hambleton, W.T.; Kawakami, E.; Amromin, E.L. Creation and maintenance of cavities under horizontal surfaces in steady and gust flows. *J. Fluids Eng.* **2009**, *131*, 11301. [CrossRef]
9. Ceccio, S.L. Friction drag reduction of external flows with bubble and gas injection. *Annu. Rev. Fluid Mech.* **2010**, *42*, 183–203. [CrossRef]
10. Lay, K.A.; Yakushiji, R.; Makiharju, S.; Perlin, M.; Ceccio, S.L. Partial cavity drag reduction at high Reynolds numbers. *J. Ship Res.* **2010**, *54*, 109–119. [CrossRef]
11. Matveev, K.I. On the limiting parameters of artificial cavitation. *Ocean Eng.* **2003**, *30*, 1179–1190. [CrossRef]
12. Amromin, E. Ships with ventilated cavitation in seaways and active flow control. *Appl. Ocean Res.* **2015**, *50*, 163–172. [CrossRef]
13. Matveev, K.I. Static control of drag-reducing air cavities with variable cavitator shape. *Int. J. Marit. Eng. RINA Trans. Part A1* **2019**, *161*, 91–98.
14. Matveev, K.I. Simplified model for unsteady air cavities under ship hulls. *J. Eng. Marit. Environ.* **2020**, *234*, 100–107. [CrossRef]
15. Butuzov, A. A Artificial cavitation flow behind a slender wedge on the lower surface of a horizontal wall. *Fluid Dyn.* **1967**, *3*, 56–58. [CrossRef]
16. Choi, J.-K.; Chahine, L. Numerical study on the behavior of air layers used for drag reduction. In Proceedings of the 28th Symposium on Naval Hydrodynamics, Pasadena, CA, USA, 12–17 September 2010.
17. Shiri, A.; Leer-Andersen, M.; Bensow, R.E.; Norbby, J. Hydrodynamics of a displacement air cavity ship. In Proceedings of the 29th Symposium on Naval Hydrodynamics, Gothenburg, Sweden, 26–31 August 2012.

18. Cucinotta, F.; Guglielmino, E.; Sfravara, F.; Strasser, C. Numerical and experimental investigation of a planing Air Cavity Ship and its layer evolution. *Ocean Eng.* **2018**, *152*, 130–144. [CrossRef]
19. Hao, W. Numerical study of the effect of ship attitude on the perform of ship with air injection in bottom cavity. *Ocean Eng.* **2019**, *186*, 106119. [CrossRef]
20. Matveev, K.I. Numerical simulation of air cavity under a simplified model-scale hull form. *J. Ocean Eng. Sci.* **2020**, *5*, 68–72. [CrossRef]
21. Ferziger, J.H.; Peric, M. *Computational Methods for Fluid Dynamics*; Springer: Berlin/Heidelberg, Germany, 1999.
22. Hirt, C.W.; Nichols, B.D. Volume of fluid (VOF) methods for the dynamics of free boundaries. *J. Comput. Phys.* **1981**, *39*, 201–225. [CrossRef]
23. Rodi, W. Experience with two-layer models combining the k-ε model with a one-equation model near the wall. In Proceedings of the 29th Aerospace Sciences Meeting, Reno, NV, USA, 7–10 January 1991.
24. STAR-CCM + Manual. 2021. Available online: https://www.plm.automation.siemens.com/global/en/products/simcenter/STAR-CCM.html (accessed on 15 March 2021).
25. Rotte, G.; Kerkvliet, M.; van Terwisga, T. Exploring the limits of RANS-VoF modeling for air cavity flows. *Int. Shipbuild. Prog.* **2019**, *66*, 273–293. [CrossRef]
26. Mukha, T.; Bensow, R.E. Flow dynamics in the closure region of an internal ship air cavity. *Ocean Eng.* **2020**, *216*, 108192. [CrossRef]
27. Roache, P.J. *Verification and Validation in Computational Science and Engineering*; Hermosa: Albuquerque, NM, USA, 1998.
28. Matveev, K.I. Three-dimensional wave patterns in long air cavities on a horizontal plane. *Ocean Eng.* **2007**, *34*, 1882–1891. [CrossRef]
29. Schmidt, G.H. Linearized stern flow of a two-dimensional shallow draft ship. *J. Ship Res.* **1981**, *25*, 236–242. [CrossRef]